Colloids and Surfaces B: Biointerfaces 224 (2023) 113211

Contents lists available at ScienceDirect

Colloids and Surfaces B: Biointerfaces

journal homepage: www.elsevier.com/locate/colsurfb

The effects of adsorbed benzo(a)pyrene on dynamic behavior of polystyrene nanoplastics through phospholipid membrane: A molecular simulation study

Shiqiang Cheng [a], Zhicheng Ye [a,*], Xiong Wang [b], Cheng Lian [a], Yazhuo Shang [a,*], Honglai Liu [a]

[a] Key Laboratory for Advanced Materials, School of Chemistry and Molecular Engineering, East China University of Science and Technology, Shanghai 200237, China
[b] Department of Dermatology, Shanghai Jiao Tong University Affiliated Sixth People's Hospital, Shanghai 200233, China

ARTICLE INFO

Keywords:
Nanoplastics
Benzo(a)pyrene
DPPC bilayer
Cytotoxicity
Molecular simulation

ABSTRACT

Nanoplastics (NPs) are mainly generated from the decomposition of plastic waste and industrial production, which have attracted much attention due to the potential risk for humans. The ability of NPs to penetrate different biological barriers has been proved, but the understanding of molecular details is very limited, especially for organic pollutant-NP combinations. Here, we investigated the uptake process of polystyrene NPs (PSNPs) combined with benzo(a)pyrene (BAP) molecules by dipalmitoylphosphatidylcholine (DPPC) bilayers by molecular dynamics (MD) simulations. The results showed that the PSNPs can adsorb and accumulate BAP molecules in water phase and then carried BAP molecules to enter DPPC bilayers. At the same time, the adsorbed BAP promoted the penetration of PSNPs into DPPC bilayers effectively by hydrophobic effect. The process of BAP-PSNP combinations penetrating into DPPC bilayers can be summarized into four steps including adhesion on the DPPC bilayer surface, uptake by the DPPC bilayer, BAP molecules detached from the PSNPs, and the PSNPs depolymerized in the bilayer interior. Furthermore, the amount of adsorbed BAP on PSNPs affected the properties of DPPC bilayers directly, especially the fluidity of DPPC bilayers that determine the physiologic function. Obviously, the combined effect of PSNPs and BAP enhanced the cytotoxicity. This work not only presented a vivid transmembrane process of BAP-PSNP combinations and revealed the nature of the effects of adsorbed benzo(a)pyrene on the dynamic behavior of polystyrene nanoplastics through phospholipid membrane, but also provide some necessary information of the potential damage for organic pollutant-nanoplastic combinations on human health at a molecular level.

1. Introduction

In recent decades, owing to excellent properties and low cost, plastics are widely used in daily life and commercial production [1]. However, only 6–26% of plastics are recycled and most are released into the environment through various pathways [2]. By 2025, 11 billion metric tons of plastics are predicted to accumulate in the environment [3]. Therefore, plastic pollution is one of the most challenging problems. Over time, plastic waste would degrade into smaller pieces through external environmental effects [4]. Generally, plastic particles less than 5 mm in size are defined as microplastics (MPs) [5], and those less than 100 nm in size are defined as nanoplastics (NPs) [6]. Moreover, NPs are also produced industrially for specific applications, such as personal care products [7,8], nanocomposites [9], and biomedicine [10,11]. The use of these daily products also can introduce NPs into the natural environment [12,13]. Therefore, people can be exposed to NPs in a variety of ways, such as inhalation, oral ingestion, or absorption by the skin [14]. Several studies have shown that NPs can be dispersed throughout the body, crossing different biological barriers and thus able to migrate and accumulate in different living organisms' tissues [15–17]. Recently, Leslie et al. reported the presence of plastic particles in the human vascular system for the first time [18]. Wu et al. also detected microplastic accumulation in thrombi [19]. These plastic particles may cause malfunction or damage to the tissues and organs in which they accumulate. Therefore, the potential hazards of ultra-fine plastic particles to human health have caused great concern.

Owing to special surface properties (hydrophobic surface and large surface area), NPs have a strong adsorption affinity for some

* Corresponding authors.
E-mail addresses: yezhicheng@ecust.edu.cn (Z. Ye), shangyazhuo@ecust.edu.cn (Y. Shang).

https://doi.org/10.1016/j.colsurfb.2023.113211
Received 8 December 2022; Received in revised form 20 January 2023; Accepted 18 February 2023
Available online 20 February 2023

hydrophobic organic compounds (HOCs) [20], such as polycyclic aromatic hydrocarbons (PAHs) [21,22] and polychlorinated biphenyls (PCBs) [23]. Some studies have shown that NPs may act as transport vehicles for these pollutants [24,25]. The absorption of organic pollutants on NPs would change their environmental transformation and bioavailability. For instance, Ji and Wang et al. demonstrate that PS nanoparticles could adsorb benzo(a)pyrene (BAP) nanoclusters and serve as a carrier that enters the cells by experiment [24]. Li et al. also demonstrate the synergistic effect of polystyrene (PS) NPs and organic contaminants on the promotion of amyloid aggregation, the results also imply that small organic contaminants could enhance the potential neurotoxicity of NPs [26]. Many organic contaminants are strongly carcinogenic and widely distributed in atmospheric or aquatic environments. For example, PAHs, are a class of toxic chemicals with more than two fused aromatic rings, which are produced by the incomplete burning of fossil fuels and widely distributed in the atmosphere [27]. Increasing evidence demonstrates that exposure to PAHs can lead to a series of health hazards, including liver toxicity, immune system suppression, and carcinogenic toxicity [28,29]. Up to now, at least three types of PAHs have been classified as carcinogens by the International Agency for Research on Cancer (IARC), including BAP [30]. Hence, PAH-NP combinations have attracted a lot of attention in human health. Once these organic pollutants are released into the organism, they may further affect the normal physiological activities of the organism, causing damage that may exceed that of NPs [26]. The combination of NPs and organic pollutants may lead to different effects, such as synergistic, antagonistic, or potentiating effects [31]. However, there are few studies about the transmembrane behavior of PAH-NP combinations in model biological membranes and the details of the interaction between PAH-NP combinations and cell membranes are yet unclear, which limits the effective protection of PAH-NP combinations against human damage to some degree. Obviously, it is crucial to evaluate the effect of organic pollutants on NPs' behavior during the uptake process by human tissue.

Cell membranes serve as the first barrier for external harmful substances to enter the organism, the exploration of the transmembrane behavior of external harmful substances through cell membranes could provide some necessary information for avoiding the potential hazards of external harmful substances to human health [32]. However, the dynamic behavior of NPs entering the cell membranes and in cell membranes is difficult to be obtained by experiments. Molecular dynamics (MD) simulation can gain a vivid insight into the above issues at the molecular level. The change in the properties of cell membranes can be obtained by MD simulation, which is widely used to study the various components' partition tendencies in the cell membrane model and the interaction mechanism with phospholipid bilayers [33–35]. Rossi et al. have studied the effect of PS nanosized particles on model biological membranes by MD simulation, and the results revealed that PS nanosized particles would easily permeate into lipid bilayers and alter the properties of the cell membrane model [36]. Bochicchio et al. have combined MD simulation and experiments to study the interactions between polystyrene chains (25 monomers) and model lipid membranes and suggested that polystyrene oligomers perturbed the membrane structure and dynamics [37]. Phosphatidylcholine (PC), as a major constituent of cell membranes, is commonly used as a model of cell membranes [38]. For instance, the dipalmitoylphosphatidylcholine (DPPC) bilayer is widely chosen as the model of cell membranes and has obtained some meaningful information about the toxicity or location of components to the cell membrane [32,39–41].

In this work, MD simulation was used to investigate the uptake process of the PSNPs combined with BAP molecules by DPPC bilayers (as shown in Fig. 1). Firstly, the formation processes of BAP-PSNP combinations were displayed at a molecular level, then the uptake behaviors of the PSNPs combined with the different numbers of BAP molecules by DPPC bilayers were investigated. Finally, the properties of DPPC bilayers including the average area per lipid (APL), the bilayer thickness

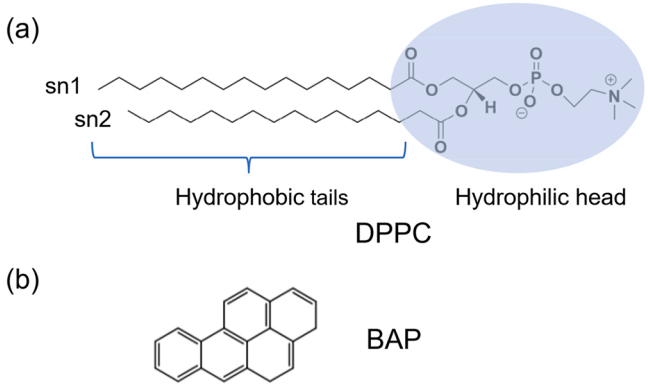

Fig. 1. Molecular structures of (a) DPPC molecule and (b) benzo(a)pyrene (BAP) molecule. Based on hydrophobicity, the DPPC molecule was here divided into two parts: the hydrophilic head and the hydrophobic tails.

(D_B), the electrostatic potentials, the lipid order parameter (S_{CD}), and the area compressibility modulus (K_A) for the systems with and without the participation of BAP-PSNP combinations were also calculated. The results not only elucidate the effect of adsorbed benzo(a)pyrene on the dynamic behavior of polystyrene nanoplastics through phospholipid membrane but also provide some necessary information for understanding the hazards of BAP-PSNP combinations on the human body.

2. Computational methods

2.1. Simulation systems setup

In this work, the PSNPs were modeled by polystyrene (PS) nanoparticles consisting of 10 short chains of polystyrene (PS10, 10 monomers). To elucidate the effect of organic pollutants (BAP molecules) on the behavior of PSNPs within cell membranes, four combinations were constructed, which were named M0 (pure PSNPs), M5 (PSNPs+5 BAP molecules), M10 (PSNPs+10 BAP molecules), and M20 (PSNPs+20 BAP molecules), respectively. To obtain the BAP-PSNP combinations as described above, we constructed a periodic box, which size was set at 6 nm × 6 nm× 6 nm. The specific number of PS10 chains and BAP molecules were randomly inserted into the simulation box and then filled with water. The isothermal and isochoric (NVT) MD simulations were performed for the constructed systems at 323 K until the formation of stable combinations.

The initial structure of the DPPC bilayer was obtained from Kukol [42]. In this work, the DPPC bilayer comprised 9759 water molecules and 128 DPPC molecules with 64 DPPC molecules in both the upper and lower leaflets. To get the well-equilibrated DPPC bilayer for the next simulations, the isothermal and isobaric (NPT) MD simulations were performed for the hydrated DPPC bilayer at 323 K for 500 ns. The final system size was 6.37 nm × 6.37 nm× 11.38 nm.

To investigate the uptake process of BAP-PSNP combinations by DPPC bilayers, the aggregates were placed into the water phase close to the upper leaflet of the DPPC bilayer and a few overlapping water molecules were removed. Five bilayer systems were constructed and detailed information on simulation systems was listed in Table S1. A system without PSNPs and BAP-PSNP combinations was constructed as the control group (PM system). All systems were submitted to 500 ns NPT MD simulation to study the uptake processes and changes of bilayer properties.

2.2. Simulation parameters

All MD simulations were performed with the GROMACS 2018.8 software package [43,44]. The structure and topology of the DPPC molecule comprising the lipid bilayer were obtained from Kukol [42].

The PS10 chains and BAP molecules were parameterized using the GROMOS96 54a7 force field [45] and the topology and coordinate files were obtained from the ATB server [46,47]. Water molecules were modeled by the simple point charge (SPC) model [48]. The temperature was kept at 323 K *via* the V-rescale thermostat [49] with a 0.2 ps coupling time constant, which was higher than the phase transition temperature of DPPC molecules [50]. The pressure was controlled at 1 bar by the Parrinello-Rahman barostat [51] with a 2.0 ps coupling time constant and compressibility of the 4.5×10^{-5} bar^{-1} with semi-isotropic coupling to obtain a tensionless bilayer. A cut-off distance of 1.0 nm was used for van der Waals and electrostatic interactions. The Particle-Mesh Ewald (PME) algorithm [52] was used to calculate long-range electrostatic interactions. The time step was 2 fs and bonds with hydrogen atoms were constrained using the LINCS algorithm [53]. Periodic boundary conditions were applied in all three dimensions. Every system was performed for 500 ns in the NPT ensemble. The simulation trajectories were saved every 20 ps. The last 50–100 ns of each simulation trajectory was used to analyze the properties of DPPC bilayers. All simulation results were visualized by the VMD program package [54].

3. Results and discussion

3.1. Formation of BAP-PSNP combinations

Both PS10 chains and BAP molecules were highly hydrophobic and contained benzene rings, they would spontaneously aggregate into a cluster owing to the hydrophobic interaction and π-π stacking interaction in water phase [20]. To clearly show the formation process of BAP and PSNP aggregates, the aggregation process was simulated. The snapshots of aggregates were shown in Fig. 2, in which four systems contained 0, 5, 10, and 20 BAP molecules, respectively. In system M0, the PSNPs were a nearly spherical cluster, whose radius was approximately 1.5 nm. For BAP-PSNP combinations, BAP molecules were mainly distributed on the surface of PSNPs, and the size increased as the number of BAP molecules increased. Further details could be found in Supporting Information (Fig. S1).

3.2. Uptake process of BAP-PSNP combinations by DPPC bilayer

For real-time monitoring of the uptake process of BAP-PSNP combinations by DPPC bilayers, the distances between the center of mass (COM) of BAP-PSNP combinations and the COM of DPPC bilayers with time evolution were recorded. Fig. 3a was an initial configuration of a representative system containing a BAP-PSNP combination. Fig. 3b was the COM distances between BAP-PSNP combinations and DPPC bilayers as the combinations moved through the membrane. At the beginning of the simulations, the COM distances between BAP-PSNP combinations and DPPC bilayers were about 4.0 nm, then the COM distances decreased as the simulations began, indicating the BAP-PSNP combinations were moving closer to the COM of DPPC bilayers. After 300 ns simulation, the COM distances all decreased to about zero and kept around zero until the end of the simulations, suggesting all the combinations had entered the core of DPPC bilayers and kept in the core of DPPC bilayers. Meanwhile, we also observed different uptake behaviors for different BAP-PSNP combinations. Comparing the M0 with the other three, the PSNPs combined with BAP molecules took less time to permeate into the core of DPPC bilayers, especially for the M20, which entered the bilayer core at ~50 ns. For the M0 and M10, a plateau existed on the COM distance profiles when the distance was about 2.0 nm. The absorption of BAP molecules increased the hydrophobicity of the PSNPs, which may assist the permeation of BAP-PSNP combinations into DPPC bilayers. However, the adsorbed BAP molecules also increased the size of BAP-PSNP combinations, which also limited the penetration of combinations into lipid bilayers to some extent.

In addition, we also investigated the uptake process of BAP alone by the DPPC bilayer without the presence of PSNPs. As shown in Fig. S2, BAP molecules were randomly dispersed in the water phase before the simulation, and all BAP molecules permeated into the interior of the DPPC bilayer within 500 ns simulation. The different numbers of BAP molecules all entered the DPPC bilayer at different moments (seeing Fig. S2 dashed circle), which was mainly due to the hydrophobic interaction between BAP and the hydrophobic tails of DPPC molecules. Compared to the transmembrane behavior of the BAP-PSNP combinations, it was found that the PSNPs also can promote the entrance and accumulation of BAP molecules in the membrane.

To visualize the uptake process of BAP-PSNP combinations by the DPPC bilayer, a series of snapshots at different moments were selected.

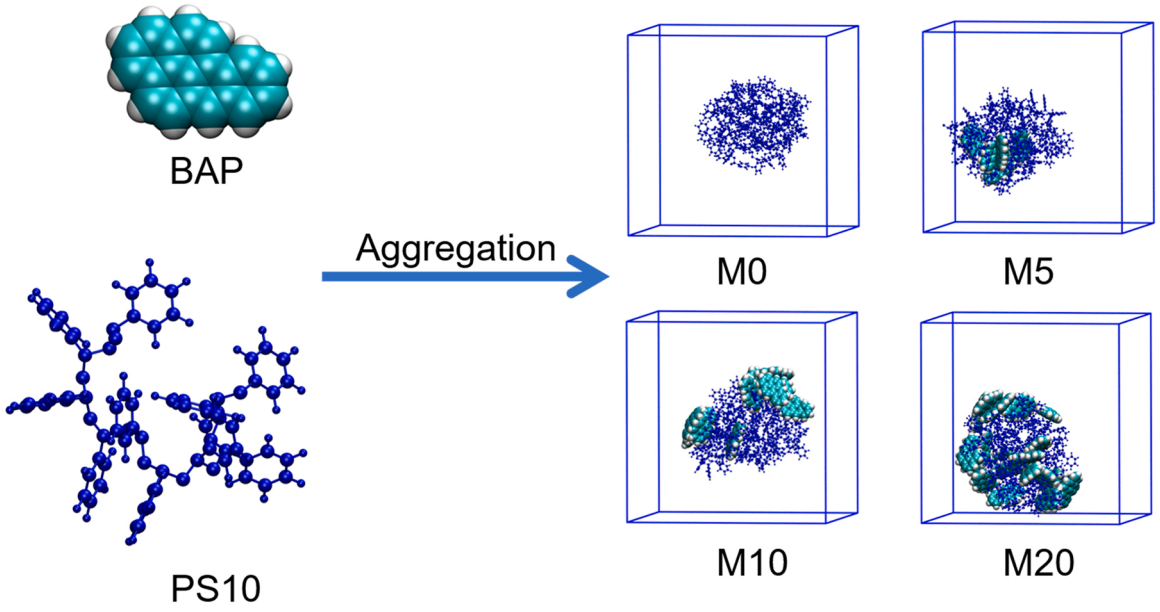

Fig. 2. Schematic diagram of the formation process of BAP-PSNP combinations. The BAP molecules and PS10 chains were shown by the VDW model and the CPK model, respectively.

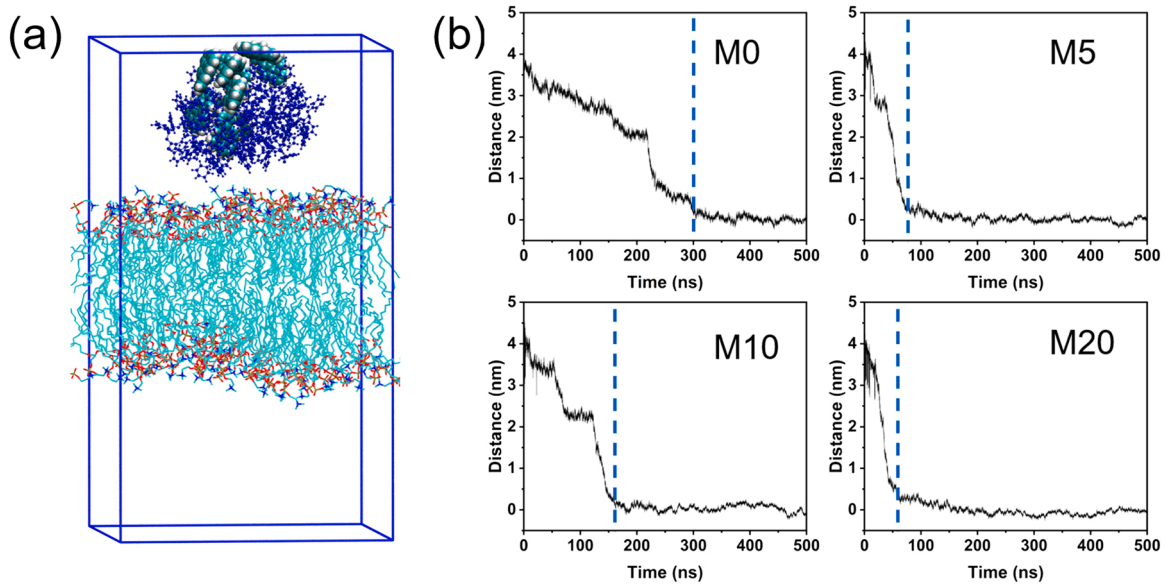

Fig. 3. (a) The initial configuration of a representative system containing a BAP-PSNP combination. Water molecules were omitted for clarity. (b) The COM distances between BAP-PSNP combinations and DPPC bilayers with time evolution in containing BAP-PSNP combination systems. The blue dashed lines corresponded to the time points at which BAP-PSNP combinations reached the center of DPPC bilayers.

As displayed in Fig. 4, at the beginning of simulations, the BAP-PSNP combinations were spherical clusters and located in the water phase. After 500 ns simulation, BAP-PSNP combinations all permeated into the interior of the DPPC bilayer. Generally speaking, the uptake progress of BAP-PSNP combinations by DPPC bilayers can be divided into four stages including the adhesion stage, intake stage, release stage as well as depolymerized stage. Once the BAP-PSNP combinations were formed (0 ns) in the aqueous phase, they would quickly approach the DPPC bilayer, and adsorbed on the surface of the DPPC bilayer compactly. When the COM distances between BAP-PSNP combinations and the

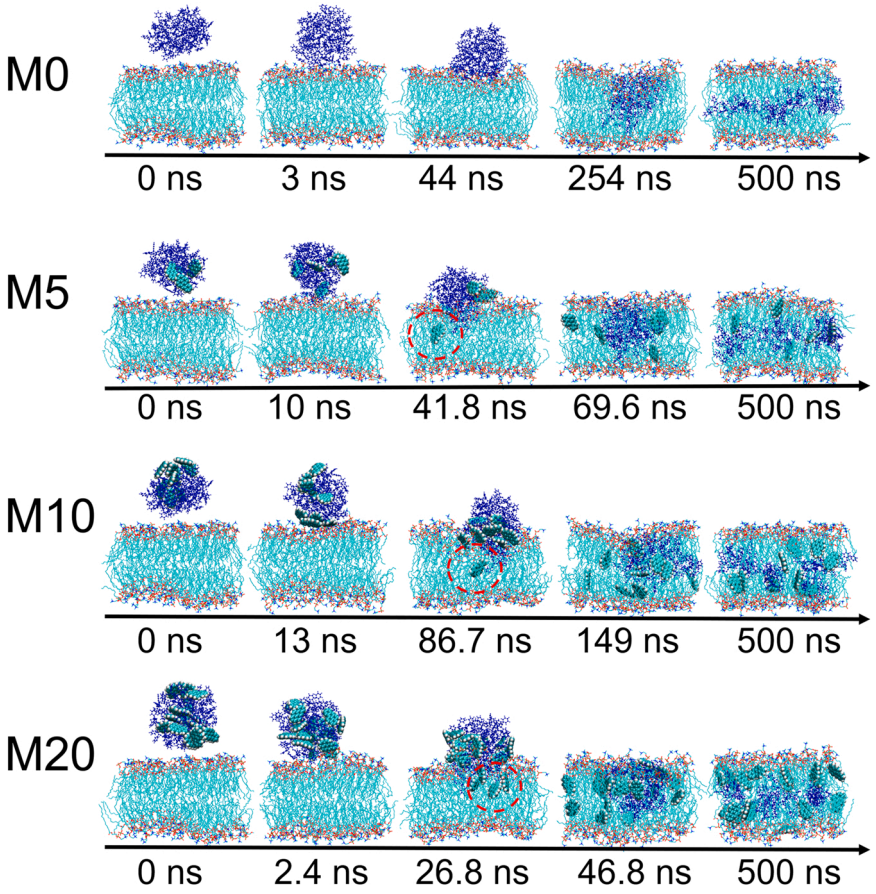

Fig. 4. The uptake process of different BAP-PSNP combinations by DPPC bilayers. Water molecules in each system were omitted for clarity.

DPPC bilayer were about 3.5 nm, the adsorption of BAP-PSNP combinations, namely, the adhesion stage was completed. Then, part of the PS10 chains composing the PSNPs tended to be inserted into the surface of the bilayer first, similar to the anchor and promoted the whole combinations to penetrate the interior of the DPPC bilayer gradually, which was the intake stage. The BAP molecules adsorbed on the surface of PSNPs started to detach and release into the interior of the bilayer once enter the bilayer, which was the release stage (as shown in Fig. 4, red circles). After the combinations completely entered the DPPC bilayer, as simulation time was extended, the PSNPs also appeared to depolymerize gradually, which was called the depolymerized stage. Bochicchio et al. have observed the same phenomenon that short polystyrene chains tend to permeate into the DPPC bilayer and dissolved in the hydrophobic core of the bilayer [37]. Meanwhile, BAP molecules were mainly located on both leaflets of the DPPC bilayer. As presented in Fig. S3, the final depolymerized phenomenon could be observed clearly. Both PS10 chains and BAP molecules were uniformly dispersed in the lateral section within the DPPC bilayer, without obvious aggregation. Furthermore, during the simulation, it was observed that when the combinations were both in the water phase and on the bilayer surface, BAP molecules were always located in the vicinity of PSNPs in a non-covalent manner, indicating the PSNPs could adsorb BAP molecules in aqueous environment and carry BAP molecules into DPPC bilayers. Namely, PSNPs act as the carrier of BAP molecules into DPPC bilayers. It can be seen that in order to minimize the risk to human health, the coexistence of PSNPs and BAP should be avoided in the environment even at a lower concentration.

To better understand the above phenomena, the interaction energies between the BAP-PSNP combinations and DPPC bilayers were calculated. The interaction energy, E, was calculated by Eqs. (1)–(3):

$$E = E_{ele} + E_{vdW} \tag{1}$$

$$E_{ele} = E_{ele}^{A+B} - E_{ele}^{A} - E_{ele}^{B} \tag{2}$$

$$E_{vdW} = E_{vdW}^{A+B} - E_{vdW}^{A} - E_{vdW}^{B} \tag{3}$$

where E_{ele}^{A+B} represents the coulomb potential of A+B complex, while E_{ele}^{A} and E_{ele}^{B} represent the coulomb potential of A and B, respectively. Similarly, E_{vdW}^{A+B} represents the Lennard-Jones potential of A+B complex, while E_{vdW}^{A} and E_{vdW}^{B} represent the Lennard-Jones potential of A and B, respectively.

Based on amphiphilicity, the DPPC molecule was divided into two parts, hydrophilic head and hydrophobic tails (Fig. 1a). The interaction energies between BAP-PSNP combinations and hydrophilic head and hydrophobic tails of DPPC molecules with time evolution were shown in the top row of Fig. 5. The values of the total interaction energy between the BAP-PSNP combinations and DPPC molecules were always negative in all systems, indicating the uptake of these combinations by DPPC bilayers was favorable from the viewpoint of thermodynamics [33]. As these combinations continuously penetrated the interior of DPPC bilayers, the interaction energy between the combinations and hydrophilic head groups of DPPC bilayers had no obvious changes, while the attraction effect between the combinations and hydrophobic tail chains of the DPPC bilayer continuously increased. The attraction effect between the combinations and the tail chains of DPPC bilayers became stronger and stronger with the increase in the number of absorbed BAP molecules. It was clear, the adsorption of BAP molecules on the PSNPs surface increased the hydrophobicity of the combinations which favored the entrance of BAP-PSNP combinations into the DPPC bilayer. It was worth noticing that the hydrophobic effect between DPPC molecules and PS10 chains and BAP molecules both increased with the entrance of combinations into the DPPC bilayer (as shown in the second row of Fig. 5), which implied that hydrophobic tails of the DPPC molecules can not only caught the PS10 chains in PSNPs but also seized the BAP molecules by stronger hydrophobic effect and leading to the detach of BAP molecules from the PSNPs firstly. Correspondingly, the decomposition of BAP-PSNP combinations within the bilayer occurred. Further, the PSNPs composed of PS10 chains decomposed gradually.

3.3. Effect of BAP-PSNP combinations on the properties of DPPC bilayers

To explore the effects of BAP-PSNP combinations on the properties of the DPPC bilayer, the distribution of BAP-PSNP combinations within the DPPC bilayer was studied by calculating the mass density profiles for all components of the simulation systems (Fig. 6). Regardless of the presence of BAP-PSNP combinations, DPPC molecules and water molecules were symmetrically distributed in all systems. As shown in Fig. 6b-e, when BAP-PSNP combinations entered the DPPC bilayer, PS10 chains were mainly concentrated in the center of the bilayer, while BAP molecules were mainly located at ± 1 nm from the center of the bilayer. Interestingly, the number of BAP molecules introduced by the PSNPs

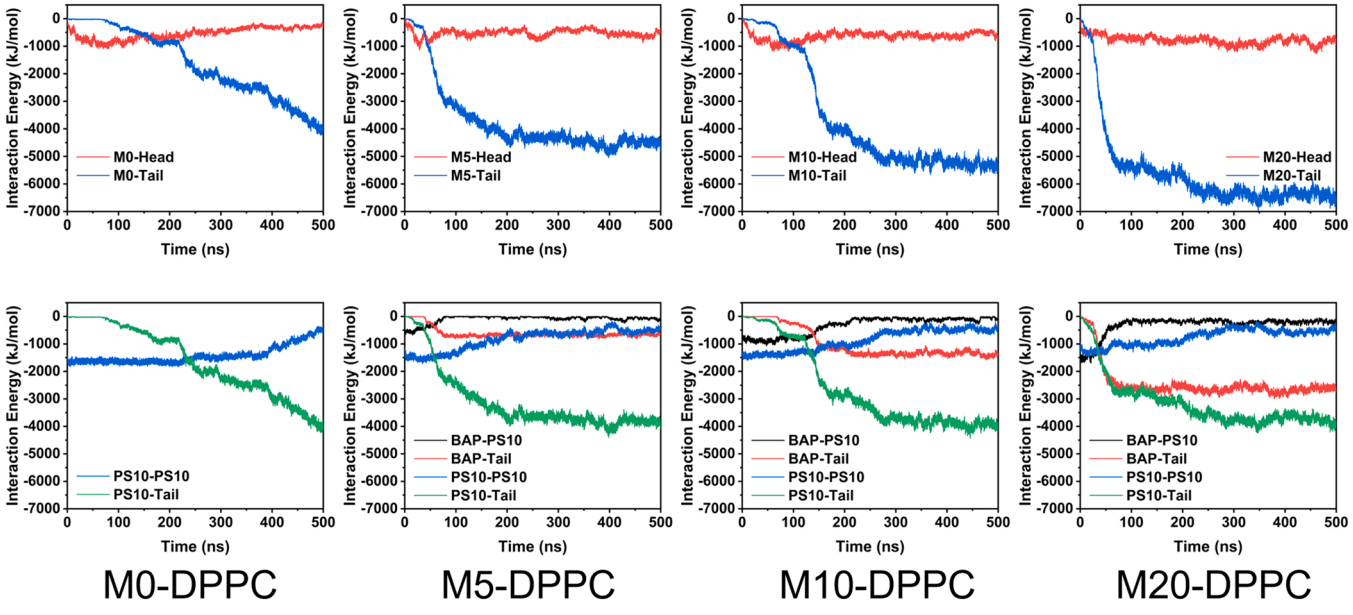

Fig. 5. The interaction energies between different components in containing BAP-PSNP combination systems.

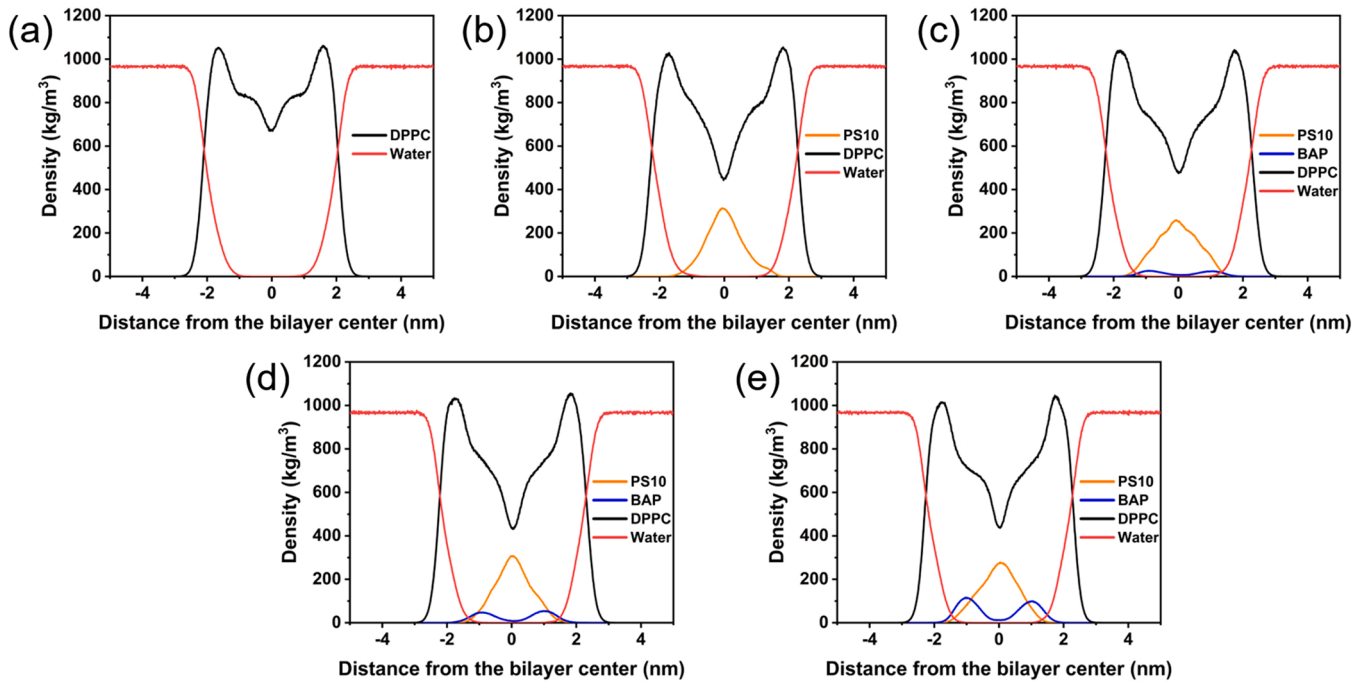

Fig. 6. Density distribution profiles of different components over the last 100 ns for all systems. (a) PM, (b) M0-DPPC system, (c) M5-DPPC system, (d) M10-DPPC system, and (e) M20-DPPC system.

almost had no effect on their preferred location in the DPPC bilayer but the introduction of BAP-PSNP combinations can result in the decrease of the density of DPPC molecules in the center of the bilayer ($Z = 0$ nm) due to the space-occupying effect of the depolymerized PS10 chains. In addition, the PS10 chains and BAP molecules can't be observed in aqueous phase, suggesting these molecules apt to stay within the bilayer. The bioaccumulation of the PSNPs and BAP molecules within cell membranes can affect the normal function of cell membranes and the combination of PSNPs and BAP molecules may lead to more severe cytotoxicity [37,55].

To further reveal the effect of BAP-PSNP combinations on the properties of the DPPC bilayer, the average area per lipid (APL), the bilayer thickness (D_B), and the area compressibility modulus (K_A) were calculated. The K_A was calculated by Eq. (4):

$$K_A = k_B T\left(A_0 / \langle (A - A_0)^2 \rangle\right) \quad (4)$$

where A_0 is the average in-plane area of the membrane, A is the in-plane area of the membrane at different times t, k_B is the Boltzmann constant, the $< >$ indicates a time average, and T is the absolute temperature. As shown in Table 1, the APL and D_B of the PM system were 0.639 nm^2 and 3.774 nm, respectively, which were consistent with the experimental results [56]. Compared with the PM system, the APL for the systems containing PSNPs and BAP-PSNP combinations all increased. In addition, the APL slightly increased with the number of absorbed BAP molecules. Similar results were also found for the bilayer thickness. All of these should be derived from the existence of the PSNPs and BAP molecules tended to enlarge the space between DPPC molecules and that of between two lipid monolayers once they entered the DPPC bilayer. Compared to the PM system, the area compressibility modulus of the M0-DPPC system decreased significantly, indicating that the PSNPs have a mechanical softening effect [36]. The additional BAP molecules also had a certain contribution to the softening effect, causing a slight increase in K_A. In summary, the PSNPs and BAP molecules affected the original structure and further affected the properties of DPPC bilayers.

Table 1
Structural and mechanical properties of DPPC bilayers for the studied systems.

System	APL (nm^2)	D_B (nm)	K_A (mN/m)
PM	0.639 ± 0.011	3.774 ± 0.064	344.7
M0-DPPC	0.653 ± 0.038	3.852 ± 0.202	120.5
M5-DPPC	0.664 ± 0.018	3.996 ± 0.121	219.2
M10-DPPC	0.666 ± 0.025	3.973 ± 0.194	142.5
M20-DPPC	0.672 ± 0.021	4.062 ± 0.168	145.7

In fact, the change of bilayer properties is also related to the interaction between hydrophilic head groups and water molecules [57,58]. The radial distribution functions (RDF) for O atoms in water molecules and P atoms in DPPC molecules were singled out to study the penetration of water molecules into the DPPC bilayer. The RDFs of O atoms around P atoms for the studied systems were shown in Fig. 7a. The variations of RDFs with the distance between O and P atoms showed a similar trend for all the studied systems, and the nearest neighbor peaks were visible at ~0.4 nm. The peak intensities of the nearest peaks for different systems followed the following order, M20-DPPC>M10-DPPC≈M5-DPPC>M0-DPPC>PM, suggesting that the PSNPs and BAP-PSNP combinations increased the interaction between O-P atom pairs and the interaction increased slightly as the number of BAP molecules increased. It was clear that the increase in APL of DPPC bilayers should be attributed to the water penetration into DPPC bilayers more deeply after DPPC bilayers ingested the PSNPs or BAP-PSNP combinations [58]. The electrostatic property of cell membranes is very important to many biological activities that are related to membrane potential, such as ion channel conduction. The electrostatic potentials of the DPPC bilayers were calculated and shown in Fig. 7b. It can be seen, the electrostatic potentials of DPPC bilayers were affected by the penetration of PSNPs or BAP-PSNP combinations. The change in the electrostatic potential would disrupt the dynamic balance of ions inside and outside the cell membrane, which would affect the normal function of the cell membrane and lead to cytotoxicity further [33,59].

The lipid order parameter is one of the most fundamental properties of lipid bilayers, which is a standard amount for evaluating the structural order of the acyl chain in the lipid bilayer. The deuterium order parameters (S_{CD}) were calculated by Eq. (5):

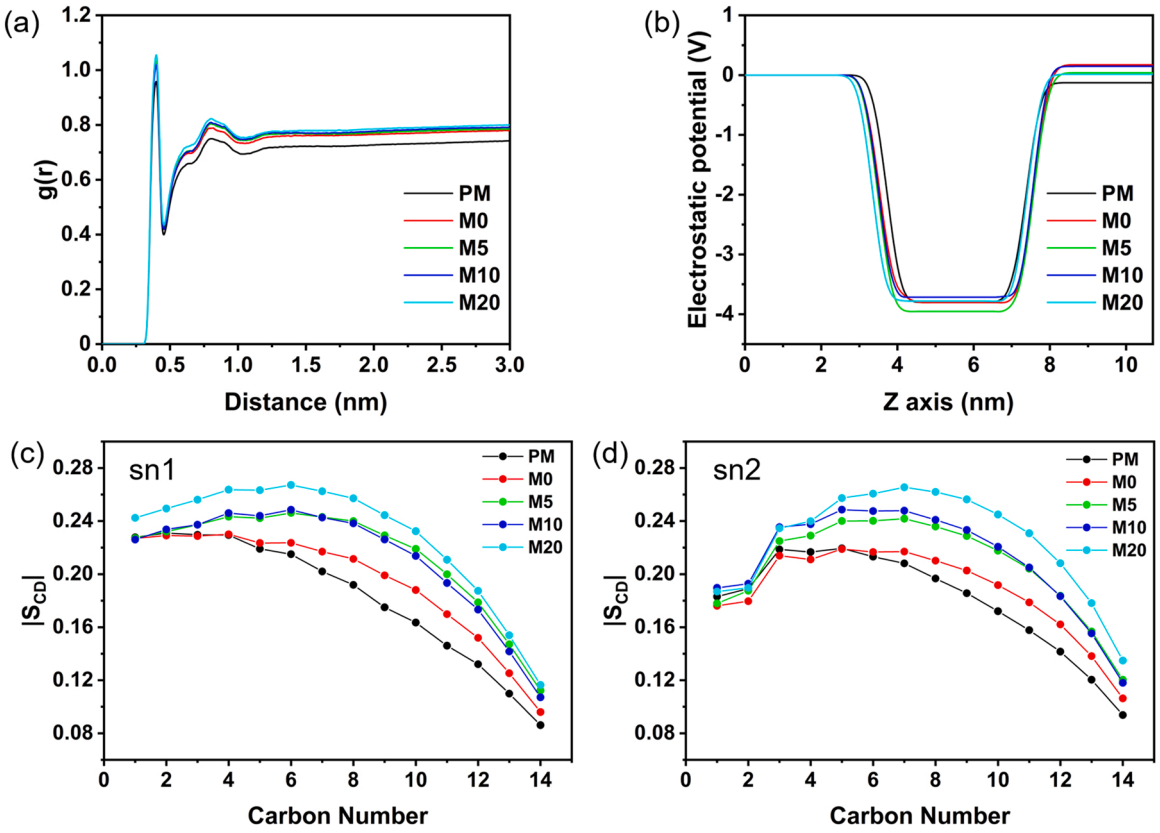

Fig. 7. (a) Radial distribution functions of P atoms in DPPC and O atoms in water. (b) Electrostatic potentials of the DPPC bilayers in the studied systems. The deuterium order parameters of (c) sn1 and (d) sn2 chains of DPPC molecules for different systems.

$$S_{CD} = \frac{3\langle \cos^2 \alpha \rangle - 1}{2} \quad (5)$$

α is the angle between the bilayer normal (Z-axis) and the C-H bond vector and the < > indicates a time average. In addition, some other properties of lipid bilayers are also related to the lipid order parameter, such as fluidity. Some experimental and computational studies have demonstrated that the increase in the order parameter of DPPC leads to a decrease in DPPC bilayer fluidity [34,60]. To reveal the effect of PSNPs and BAP-PSNP combinations on the ordering of the acyl chain structure of DPPC bilayers, the deuterium order parameters ($|S_{CD}|$) of the two acyl chains (sn1 and sn2, as shown in Fig. 1a) were selected as the studied objects. The results had shown that the deuterium order parameters of the two acyl chains showed a similar trend with the increase of BAP content (as shown in Fig. 7c and Fig. 7d). Here, the sn1 chains of DPPC molecules had been analyzed as an example. The values of $|S_{CD}|$ decreased from carbons closing to the head group region to the tail region of DPPC molecules for the pure membrane system. As can be seen that the values of $|S_{CD}|$ increased obviously for the carbons closing the tail region of DPPC in the M0-DPPC system, indicating the bioaccumulation of the PSNPs within the DPPC bilayer increased the order of the tail chains and leading to the decrease of membrane fluidity. In addition, the values of $|S_{CD}|$ displayed a greater increase in the middle region of DPPC molecules with the increase in the number of BAP molecules adsorbed by the PSNPs, which was mainly due to the characteristic accumulation of BAP within the DPPC bilayer (as shown in Fig. 6). An obvious increase of the values of $|S_{CD}|$ was also observed near the head group region in the M20-DPPC system. BAP molecules had a dose-dependent effect on the increase in the order of the tails in DPPC bilayers, implying that BAP may have a combined effect with the PSNPs and cause the decrease of membrane fluidity. In brief, the systems containing BAP-PSNP combinations led to a more significant increase in the order parameters of the DPPC bilayer, and thus the fluidity of the membrane decreased dramatically. Generally, membrane fluidity can maintain the normal physiological activities of cells and it is very important to cell membranes [61]. Therefore, the changes in membrane fluidity caused by the participation of BAP-PSNP combinations may lead to more severe cytotoxicity.

4. Conclusion

In this work, the uptake process of BAP-PSNP combinations by DPPC bilayers and their combined effects on the DPPC bilayer were studied by MD simulations. The results showed that the BAP molecules can be adsorbed and accumulated on PSNPs and form BAP-PSNP combinations in water phase. The absorption of BAP molecules promoted the permeation of BAP-PSNP combinations into DPPC bilayers due to the stronger hydrophobic interaction between BAP-PSNP combinations and the hydrophobic tail chains of DPPC compared to the pure PSNPs. The uptake process of BAP-PSNP combinations by DPPC bilayers was complicated, including the adhesion of combinations on the DPPC bilayer surface, uptake by DPPC bilayer, BAP molecules detached from PSNPs, and the PSNPs depolymerized in the bilayer interior. The uptake of the PSNPs or BAP-PSNP combinations by DPPC bilayers affected the properties of the bilayer, including the distribution of DPPC molecules, the structural order of the acyl chains in the lipid bilayer as well as the electrostatic potentials of DPPC bilayers. Correspondingly, the fluidity of membrane decreased significantly, which cause more severe cytotoxicity. Our study highlights the uptake process and harmful effects of organic pollutants adsorbed on the surface of polystyrene nanoplastics on the cell membrane model, which can promote the understanding of potential risks and cytotoxicity of nanoplastics in the natural environment.

CRediT authorship contribution statement

Shiqiang Cheng: Conceptualization, Methodology, Investigation, Writing – original draft. **Zhicheng Ye:** Methodology. **Xiong Wang:** Methodology. **Cheng Lian:** Methodology. **Yazhuo Shang:** Supervision, Resources, Writing – review & editing. **Honglai Liu:** Supervision.

Declaration of Competing Interest

The authors declare that they have no known competing financial interests or personal relationships that could have appeared to influence the work reported in this paper.

Data Availability

The authors do not have permission to share data.

Acknowledgments

We acknowledge the financial support of this work by the Fundamental Research Funds for the Central Universities (2022ZFJH004) and the National Natural Science Foundation of China for Innovative Research Groups (No. 51621002).

Appendix A. Supporting information

Detailed information of simulation systems (Table S1); The structures and sizes of different BAP-PSNP combinations (Fig. S1); The uptake process of different numbers of BAP alone by DPPC bilayers (Fig. S2); Top view of the final snapshots in different systems containing BAP-PSNP combinations (Fig. S3).

Appendix B. Supporting information

Supplementary data associated with this article can be found in the online version at doi:10.1016/j.colsurfb.2023.113211.

References

[1] N.N. Phuong, A. Zalouk-Vergnoux, L. Poirier, A. Kamari, A. Châtel, C. Mouneyrac, F. Lagarde, Is there any consistency between the microplastics found in the field and those used in laboratory experiments? Environ. Pollut. 211 (2016) 111–123.
[2] O.S. Alimi, J. Farner Budarz, L.M. Hernandez, N. Tufenkji, Microplastics and nanoplastics in aquatic environments: aggregation, deposition, and enhanced contaminant transport, Environ. Sci. Technol. 52 (2018) 1704–1724.
[3] J. Brahney, M. Hallerud, E. Heim, M. Hahnenberger, S. Sukumaran, Plastic rain in protected areas of the United States, Science 368 (2020) 1257–1260.
[4] J.P. da Costa, P.S.M. Santos, A.C. Duarte, T. Rocha-Santos, Nano)plastics in the environment – sources, fates and effects, Sci. Total Environ. 566–567 (2016) 15–26.
[5] S. Dong, M. Qu, Q. Rui, D. Wang, Combinational effect of titanium dioxide nanoparticles and nanopolystyrene particles at environmentally relevant concentrations on nematode Caenorhabditis elegans, Ecotoxicol. Environ. Saf. 161 (2018) 444–450.
[6] S. Xie, A. Zhou, T. Wei, S. Li, B. Yang, G. Xu, J. Zou, Nanoplastics induce more serious microbiota dysbiosis and inflammation in the gut of adult zebrafish than microplastics, Bull. Environ. Contam. Toxicol. 107 (2021) 640–650.
[7] L.S. Fendall, M.A. Sewell, Contributing to marine pollution by washing your face: microplastics in facial cleansers, Mar. Pollut. Bull. 58 (2009) 1225–1228.
[8] L.M. Hernandez, N. Yousefi, N. Tufenkji, Are there nanoplastics in your personal care products? Environ. Sci. Technol. Lett. 4 (2017) 280–285.
[9] S. Sharma, S. Chatterjee, Microplastic pollution, a threat to marine ecosystem and human health: a short review, Environ. Sci. Pollut. Res. 24 (2017) 21530–21547.
[10] R.M. Urban, J.J. Jacobs, M.J. Tomlinson, J. Gavrilovic, J. Black, M. Peoc'h, Dissemination of wear particles to the liver, spleen, and abdominal lymph nodes of patients with hip or knee replacement*, JBJS 82 (2000).
[11] M. Oliveira, M. Almeida, I. Miguel, A micro(nano)plastic boomerang tale: a never ending story, TrAC Trends Anal. Chem. 112 (2019) 196–200.
[12] Y. Yang, Q. Wu, D. Wang, Epigenetic response to nanopolystyrene in germline of nematode Caenorhabditis elegans, Ecotoxicol. Environ. Saf. 206 (2020), 111404.
[13] M.T. Ekvall, M. Lundqvist, E. Kelpsiene, E. Šileikis, S.B. Gunnarsson, T. Cedervall, Nanoplastics formed during the mechanical breakdown of daily-use polystyrene products, Nanoscale Adv. 1 (2019) 1055–1061.
[14] R. Lehner, C. Weder, A. Petri-Fink, B. Rothen-Rutishauser, Emergence of nanoplastic in the environment and possible impact on human health, Environ. Sci. Technol. 53 (2019) 1748–1765.
[15] C.M. Boerger, G.L. Lattin, S.L. Moore, C.J. Moore, Plastic ingestion by planktivorous fishes in the North Pacific Central Gyre, Mar. Pollut. Bull. 60 (2010) 2275–2278.
[16] M.A. Browne, A. Dissanayake, T.S. Galloway, D.M. Lowe, R.C. Thompson, Ingested microscopic plastic translocates to the circulatory system of the mussel, Mytilus edulis (L.), Environ. Sci. Technol. 42 (2008) 5026–5031.
[17] M. Mistri, A.A. Sfriso, E. Casoni, M. Nicoli, C. Vaccaro, C. Munari, Microplastic accumulation in commercial fish from the Adriatic Sea, Mar. Pollut. Bull. 174 (2022), 113279.
[18] H.A. Leslie, M.J.M. van Velzen, S.H. Brandsma, A.D. Vethaak, J.J. Garcia-Vallejo, M.H. Lamoree, Discovery and quantification of plastic particle pollution in human blood, Environ. Int. 163 (2022), 107199.
[19] D. Wu, Y. Feng, R. Wang, J. Jiang, Q. Guan, X. Yang, H. Wei, Y. Xia, Y. Luo, Pigment microparticles and microplastics found in human thrombi based on Raman spectral evidence, J. Adv. Res. (2022).
[20] C.M. Rochman, C. Manzano, B.T. Hentschel, S.L.M. Simonich, E. Hoh, Polystyrene plastic: a source and sink for polycyclic aromatic hydrocarbons in the marine environment, Environ. Sci. Technol. 47 (2013) 13976–13984.
[21] X. Tan, X. Yu, L. Cai, J. Wang, J. Peng, Microplastics and associated PAHs in surface water from the Feilaixia Reservoir in the Beijiang River, China, Chemosphere 221 (2019) 834–840.
[22] L. Sørensen, E. Rogers, D. Altin, I. Salaberria, A.M. Booth, Sorption of PAHs to microplastic and their bioavailability and toxicity to marine copepods under co-exposure conditions, Environ. Pollut. 258 (2020), 113844.
[23] I. Velzeboer, C.J.A.F. Kwadijk, A.A. Koelmans, Strong sorption of PCBs to nanoplastics, microplastics, carbon nanotubes, and fullerenes, Environ. Sci. Technol. 48 (2014) 4869–4876.
[24] Y. Ji, Y. Wang, D. Shen, Q. Kang, J. Ma, L. Chen, Revisiting the cellular toxicity of benzo[a]pyrene from the view of nanoclusters: size- and nanoplastic adsorption-dependent bioavailability, Nanoscale 13 (2021) 1016–1028.
[25] A.A. Koelmans, A. Bakir, G.A. Burton, C.R. Janssen, Microplastic as a vector for chemicals in the aquatic environment: critical review and model-supported reinterpretation of empirical studies, Environ. Sci. Technol. 50 (2016) 3315–3326.
[26] C. Li, Y. Ma, X. Liu, R. Huang, R. Su, W. Qi, J. Che, Z. He, Synergistic effect of polystyrene nanoplastics and contaminants on the promotion of insulin fibrillation, Ecotoxicol. Environ. Saf. 214 (2021), 112115.
[27] K.J. Nam, Q. Li, S.K. Heo, S. Tariq, J. Loy-Benitez, T.Y. Woo, C.K. Yoo, Inter-regional multimedia fate analysis of PAHs and potential risk assessment by integrating deep learning and climate change scenarios, J. Hazard. Mater. 411 (2021), 125149.
[28] Q. Shi, R.R. Fijten, D. Spina, Y. Riffo Vasquez, V.M. Arlt, R.W. Godschalk, F.J. Van Schooten, Altered gene expression profiles in the lungs of benzo[a]pyrene-exposed mice in the presence of lipopolysaccharide-induced pulmonary inflammation, Toxicol. Appl. Pharmacol. 336 (2017) 8–19.
[29] Y. Cao, L. Zhang, Y. Geng, Y. Li, Q. Zhao, J. Huang, P. Ning, S. Tian, Evaluation of the permeability and potential toxicity of polycyclic aromatic hydrocarbons to pulmonary surfactant membrane by the parallel artificial membrane permeability assay model, Chemosphere 290 (2022), 132485.
[30] B. Ewa, M.-Š. Danuta, Polycyclic aromatic hydrocarbons and PAH-related DNA adducts, J. Appl. Genet. 58 (2017) 321–330.
[31] J. Bhagat, N. Nishimura, Y. Shimada, Toxicological interactions of microplastics/nanoplastics and environmental contaminants: current knowledge and future perspectives, J. Hazard. Mater. 405 (2021), 123913.
[32] W. Wang, J. Zhang, Z. Qiu, Z. Cui, N. Li, X. Li, Y. Wang, H. Zhang, C. Zhao, Effects of polyethylene microplastics on cell membranes: a combined study of experiments and molecular dynamics simulations, J. Hazard. Mater. 429 (2022), 128323.
[33] S. Yuan, H. Zhang, X. Wang, H. Zhang, Z. Zhang, S. Yuan, Molecular insights into the uptake of SiO2 nanoparticles on phospholipid membrane: effect of surface properties and particle size, Colloids Surf. B: Biointerfaces 210 (2022), 112250.
[34] M.A.A. Ayee, C.W. Roth, B.S. Akpa, Structural perturbation of a dipalmitoylphosphatidylcholine (DPPC) bilayer by warfarin and its bolaamphiphilic analogue: a molecular dynamics study, J. Colloid Interface Sci. 468 (2016) 227–237.
[35] Y. Yuan, X. Liu, T. Liu, W. Liu, Y. Zhu, H. Zhang, C. Zhao, Molecular dynamics exploring of atmosphere components interacting with lung surfactant phospholipid bilayers, Sci. Total Environ. 743 (2020), 140547.
[36] G. Rossi, J. Barnoud, L. Monticelli, Polystyrene nanoparticles perturb lipid membranes, J. Phys. Chem. Lett. 5 (2014) 241–246.
[37] D. Bochicchio, L. Cantu, M.V. Cadario, L. Palchetti, F. Natali, L. Monticelli, G. Rossi, E. Del Favero, Polystyrene perturbs the structure, dynamics, and mechanical properties of DPPC membranes: An experimental and computational study, J. Colloid Interface Sci. 605 (2022) 110–119.
[38] Z. Cui, M. Houweling, Phosphatidylcholine and cell death, Biochim. Et. Biophys. Acta (BBA) - Mol. Cell Biol. Lipids 1585 (2002) 87–96.
[39] J. Chen, D. Mao, X. Wang, G. Zhou, S. Zeng, L. Chen, C. Dai, S. Feng, Encapsulation and release of drug molecule pregabalin based on ultrashort single-walled carbon nanotubes, J. Phys. Chem. C. 123 (2019) 9567–9574.
[40] Z. Xue, Q. Sun, L. Zhang, Z. Kang, L. Liang, Q. Wang, J.-W. Shen, Graphene quantum dot assisted translocation of drugs into a cell membrane, Nanoscale 11 (2019) 4503–4514.
[41] Y. Liu, X. Pang, J. Song, X. Liu, J. Song, Y. Yuan, C. Zhao, Exploring the membrane toxicity of decabromodiphenyl ethane (DBDPE): Based on cell membranes and lipid membranes model, Chemosphere 216 (2019) 524–532.

[42] A. Kukol, Lipid models for united-atom molecular dynamics simulations of proteins, J. Chem. Theory Comput. 5 (2009) 615–626.
[43] H.J.C. Berendsen, D. van der Spoel, R. van Drunen, GROMACS: a message-passing parallel molecular dynamics implementation, Comput. Phys. Commun. 91 (1995) 43–56.
[44] M.J. Abraham, T. Murtola, R. Schulz, S. Páll, J.C. Smith, B. Hess, E. Lindahl, GROMACS: high performance molecular simulations through multi-level parallelism from laptops to supercomputers, SoftwareX 1–2 (2015) 19–25.
[45] N. Schmid, A.P. Eichenberger, A. Choutko, S. Riniker, M. Winger, A.E. Mark, W. F. van Gunsteren, Definition and testing of the GROMOS force-field versions 54A7 and 54B7, Eur. Biophys. J. 40 (2011) 843–856.
[46] A.K. Malde, L. Zuo, M. Breeze, M. Stroet, D. Poger, P.C. Nair, C. Oostenbrink, A. E. Mark, An automated force field topology builder (ATB) and repository: version 1.0, J. Chem. Theory Comput. 7 (2011) 4026–4037.
[47] M. Stroet, B. Caron, K.M. Visscher, D.P. Geerke, A.K. Malde, A.E. Mark, Automated topology builder version 3.0: prediction of solvation free enthalpies in water and hexane, J. Chem. Theory Comput. 14 (2018) 5834–5845.
[48] H.J.C. Berendsen, J.P.M. Postma, W.F. van Gunsteren, J. Hermans, Interaction models for water in relation to protein hydration, in: B. Pullman (Ed.), Intermolecular Forces: Proceedings of the Fourteenth Jerusalem Symposium on Quantum Chemistry and Biochemistry Held in Jerusalem, Israel, April 13–16, 1981, Springer, Netherlands, Dordrecht, 1981, pp. 331–342.
[49] G. Bussi, D. Donadio, M. Parrinello, Canonical sampling through velocity rescaling, The, J. Chem. Phys. 126 (2007), 014101.
[50] O. Berger, O. Edholm, F. Jähnig, Molecular dynamics simulations of a fluid bilayer of dipalmitoylphosphatidylcholine at full hydration, constant pressure, and constant temperature, Biophys. J. 72 (1997) 2002–2013.
[51] M. Parrinello, A. Rahman, Polymorphic transitions in single crystals: a new molecular dynamics method, J. Appl. Phys. 52 (1981) 7182–7190.
[52] T.A. Darden, D.M. York, L.G. Pedersen, Particle mesh Ewald: an N·log(N) method for Ewald sums in large systems, J. Chem. Phys. 98 (1993) 10089–10092.
[53] B. Hess, H. Bekker, H.J.C. Berendsen, J.G.E.M. Fraaije, LINCS: a linear constraint solver for molecular simulations, J. Comput. Chem. 18 (1997).
[54] W. Humphrey, A. Dalke, K. Schulten, VMD: visual molecular dynamics, J. Mol. Graph. 14 (1996) 33–38.
[55] M. Zhou, H. Yang, H. Li, L. Gu, Y. Zhou, M. Li, The effects of molecular weight and orientation on the membrane permeation and partitioning of polycyclic aromatic hydrocarbons: a computational study, Phys. Chem. Chem. Phys. 24 (2022) 2158–2166.
[56] J.F. Nagle, Area/lipid of bilayers from NMR, Biophys. J. 64 (1993) 1476–1481.
[57] V. Chaban, Computationally efficient prediction of area per lipid, Chem. Phys. Lett. 616–617 (2014) 25–29.
[58] K. Azizi, M.G. Koli, Molecular dynamics simulations of oxprenolol and propranolol in a DPPC lipid bilayer, J. Mol. Graph. Model. 64 (2016) 153–164.
[59] R.R. Arvizo, O.R. Miranda, M.A. Thompson, C.M. Pabelick, R. Bhattacharya, J. D. Robertson, V.M. Rotello, Y.S. Prakash, P. Mukherjee, Effect of nanoparticle surface charge at the plasma membrane and beyond, Nano Lett. 10 (7) (2010) 2543–2548.
[60] K. Tsuda, Association of resistin with impaired membrane fluidity of red blood cells in hypertensive and normotensive men: an electron paramagnetic resonance study, Heart Vessels 31 (2016) 1724–1730.
[61] E. Lopez-Rodriguez, J. Pérez-Gil, Structure-function relationships in pulmonary surfactant membranes: from biophysics to therapy, Biochimica et Biophysica Acta (BBA), Biomembranes 2014 (1838) 1568–1585.